analytical chemistry

pubs.acs.org/ac Article

Hemin-DNA Switch-Assisted Microfluidic Chemiluminescence Immunoimaging for Rapid and Quantitative Screening of Specific Hybridomas

Wencheng Xiao,[†] Hang Ao,[†] Nilin Wu, Jun Sun, Wenrui Hu, Yunlong Chen, Jie Wu,* and Huangxian Ju*

Cite This: *Anal. Chem.* 2026, 98, 2541−2549 Read Online

ACCESS | Metrics & More | Article Recommendations | Supporting Information

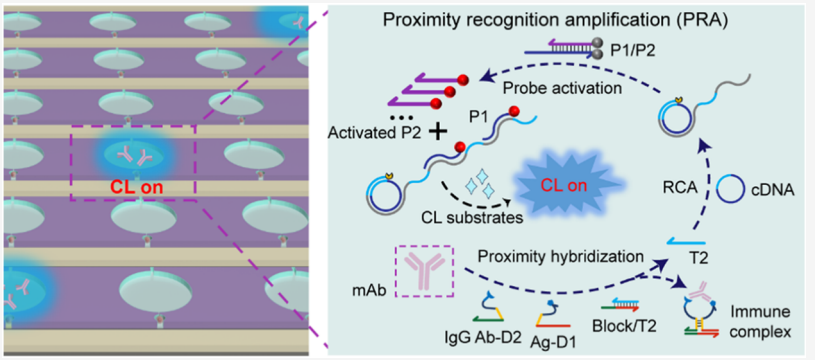

ABSTRACT: Highly sensitive detection of cell secretions at the single-cell level is critical for efficient cell screening and monoclonal antibody (mAb) production. Herein, we present a highly sensitive microfluidic chemiluminescence immunoimaging (μCLII) method for rapid and quantitative screening of high-yield specific hybridoma cells (HSHCs) by detecting single-cell secreted antibodies on a rationally designed lantern-shaped microchamber array chip. This method can effectively capture and isolate single hybridoma cells to *in situ* detect their secreted antibody by visual CL imaging with a proximity recognition amplification strategy. The proposed strategy can be performed by antibody-triggered proximity hybridization to release a DNA sequence, which initiates a rolling circle amplification reaction to turn on abundant hemin-DNA enzymes for generating strong CL emission of the imidazole-enhanced luminol-H_2O_2 system. This method shows a detection limit of ~60 antibodies per chamber, and thus enables a precise sorting of HSHCs within 70 min. Using antiproprotein convertase subtilisin/kexin type 9 mAb (PCSK9-mAb) as a model, all of the cells selected by the μCLII method show high-producing hybridomas with PCSK9-mAb yield more than 80 fg during the screening process, indicating a promising potential of the proposed method for single-cell analysis and mAbs screening.

INTRODUCTION

The rapidly developing monoclonal antibody (mAb) drugs represent the largest category within biopharmaceuticals nowadays, with a wide variety of applications in fields such as life science and healthcare.[1−3] However, the production of mAbs is time-consuming, labor-intensive, and costly, primarily due to the lack of efficient screening technologies for achieving high-yield specific hybridoma cells (HSHCs).[4,5] The most widely used screening technique is the serial-dilution method coupled with an enzyme-linked immunosorbent assay (ELISA) for mAb detection. Due to the limited sensitivity of ELISA, this method entails a lengthy process of at least one month to obtain HSHCs, as it requires multiple rounds of screening, with each round involving 1−2 weeks of clonal proliferation to obtain sufficient secreted antibodies for ELISA detection.[6−8] Therefore, the design of highly sensitive immunoassay methods enabling single-cell secreted mAb detection and quick screening of HSHCs is of great value to improve the industrial production of mAb.

Owing to the unique advantages in high-throughput single-cell manipulation,[9,10] microfluidics has recently attracted considerable attention in mAb production. Microfluidics is charming in hybridoma cell screening due to its integration with single-cell analysis for the detection of mAb secreted from single cells in picoliter chambers, where the antibody concentration can reach μg mL^{-1} level within a few hours.[11] Typical microfluidic screening methods of hybridoma cells

Received: November 25, 2025
Revised: January 6, 2026
Accepted: January 6, 2026
Published: January 14, 2026

https://doi.org/10.1021/acs.analchem.5c07461
Anal. Chem. 2026, 98, 2541−2549

Scheme 1. Schematic Diagram of (A) Screening Procedure of High-Yield Specific Hybridoma Cells (HSHCs) by Microfluidic Chemiluminescence Immunoimaging (μCLII) Platform, (B) Cell Flow Paths (i), Cell Capture (ii), Isolation (iii), and Solution Reinjection (iv), and (C) Detection of Secreted Antibody with Proximity Recognition Amplification in Individual Microchambers

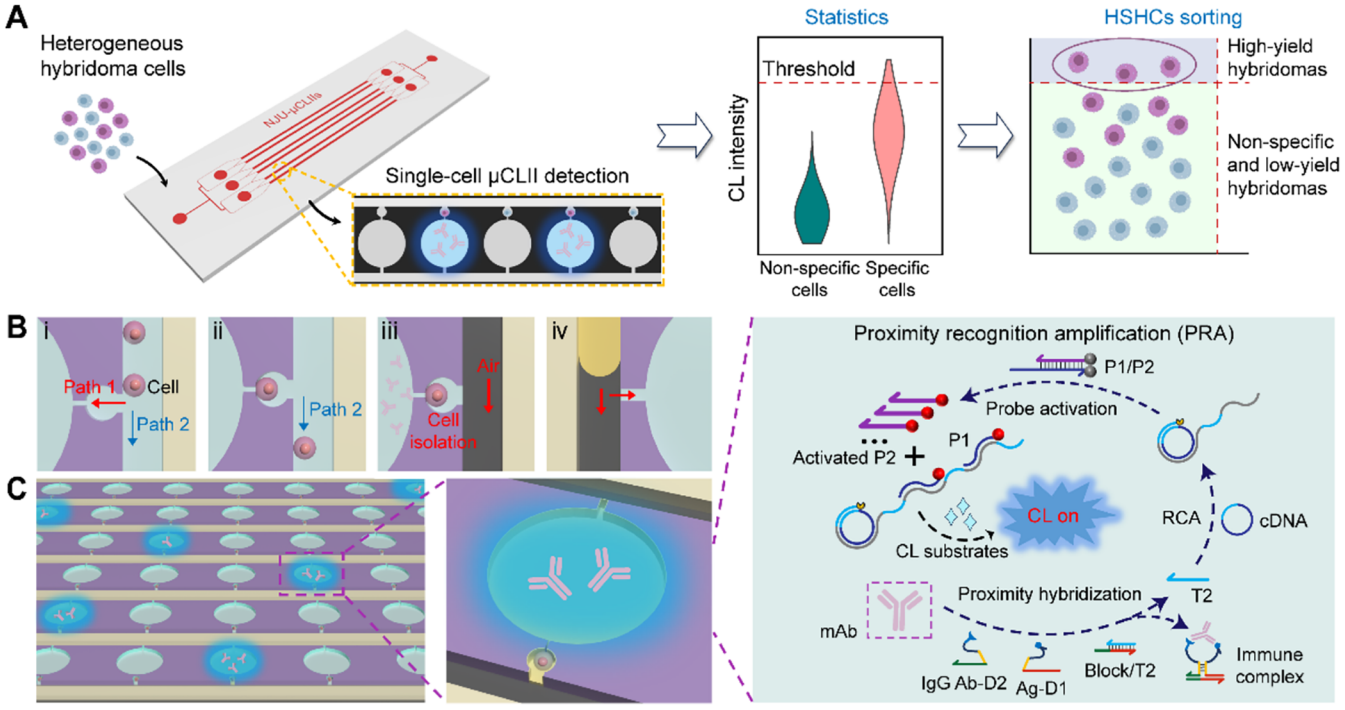

include droplet-,[12−14] microwell-,[15] and microtrap-based microfluidics.[16] The droplet-based method can generate continuous microdroplets for high-throughput single-cell encapsulation, but it suffers from Poisson distribution, and thus leads to a high probability to form empty or multiple-cell droplets, greatly reducing single-cell isolation efficiency.[17] Meanwhile, the low single-cell loading efficiency of the microwell-based method limits its practical application.[18] Although the microtrap-based method based on physical structures and liquid flow exhibits a high single-cell loading rate,[19] the developed microtrap-based methods are usually integrated with heterogeneous fluorescence immunoassays to detect antibodies secreted by single cells, which leads to the drawbacks of tedious washing steps, complex chip interface modification, signal cross-talk, and high false positives.[20−23] Therefore, it is necessary to develop other detection techniques, such as chemiluminescence (CL) imaging, for the rapid and quantitative microfluidic screening of specific hybridomas.

CL imaging possesses extremely low background and high detection sensitivity due to its ability to avoid interference from stray excitation light and biological autofluorescence.[24,25] Currently, the CL immunoassay has become one of the most advanced and widely used antibody detection methods in clinical diagnosis and biomedical research.[26,27] Besides, the CL array-based large area imaging makes it particularly suitable for high-throughput individual cell detection.[28] However, the CL array-based detection commonly is a heterogeneous assay based on the horseradish peroxidase-catalyzed luminol-H_2O_2 system.[29] Proximity immunoassay is an emerging nucleic-acid-assisted homogeneous immunoassay method. It utilizes a pair of antibody-DNA probes to recognize target proteins and generates signals through a proximal nucleic acid assembly. This design enables homogeneous detection and facilitates integration with mature DNA amplification technologies, paving the way for the development of simple and highly sensitive homogeneous immunoassays. For example, by designing proximity immunoassay with polymerase chain reaction amplification, a proteomic liquid biopsy platform with attomolar sensitivity has been reported.[30] Nevertheless, the development of a highly sensitive homogeneous CL immunoassay remains a challenge for ultralow concentration detection of cell-secreted antibody on a microfluidic chip.

In this work, we presented a microfluidic CL immunoimaging (μCLII) method for quick screening of HSHCs by detecting single-cell secreted antibodies on a lantern-shaped microchamber array chip with a newly designed proximity recognition amplification (PRA) strategy (Scheme 1A). In PRA, every antibody-triggered proximity hybridization could release a DNA sequence to initiate a rolling circle amplification (RCA) reaction for turning on abundant hemin-DNA switches, leading to a strong CL emission of the luminol-H_2O_2 system. By defining a signal threshold through statistical analysis of CL intensities of various specific and nonspecific secretors, the μCLII could achieve a 100% screening precision of HSHCs within 70 min due to the detection limit down to ~60 antibodies per chamber. Its simplicity and universality demonstrate promising applications in specific cell screening and high-purity mAb production.

EXPERIMENTAL SECTION

Materials and Reagents

Negative photoresist SU-8 3025 was obtained from MicroChem Corp., Ltd. Poly(dimethylsiloxane) (PDMS, Sylgard 184) prepolymer and curing agent were from Dow Corning Corp., Ltd. Chrome mask and 4 in. silicon wafers were supplied by Suzhou Research Materials

https://doi.org/10.1021/acs.analchem.5c07461
Anal. Chem. 2026, 98, 2541−2549

Microtech Co., Ltd. (China). Human PCSK9, PCSK9-mAb (clone number: 6A6), 6A6 hybridoma cells, human NT-proBNP, NT-proBNP-mAb (clone number: 3H2), and 3H2 hybridoma cells were from FANTIBODY (Chongqing, China). 6A6 and 3H2 hybridoma cell lines were cultured in Dulbecco's modified Eagle's medium (DMEM) supplemented with 10% fetal bovine serum and 1% penicillin-streptomycin at 37 °C with 5% CO_2. Rabbit antimouse IgG Ab was obtained from Abcam PLC Co., Ltd. DNA oligonucleotides were obtained from Sangon Bio Co., Ltd. (Shanghai, China) and TaKaRa Bio Co., Ltd. (Dalian, China), and their sequences are listed in Supporting Table S1. Phi 29 DNA polymerase, dNTPs, exonuclease I (Exo I, 20 U μL^{-1}), exonuclease III (Exo III, 100 U μL^{-1}), and corresponding buffers were obtained from New England BioLabs. Succinimidyl-trans-4-(*N*-maleimidomethyl)cyclohexane-1-carboxylate (SMCC) was obtained from Shanghai Aladdin Biochemical Technology Co., Ltd. (Shanghai, China). Luminol, tris(2-carboxyethyl) phosphine hydrochloride (TCEP) and imidazole were from Sigma-Aldrich Co., Ltd. Rapid T4 DNA ligase kit and calcein AM/propidium iodide (PI) cell viability/cytotoxicity detection kit were purchased from Beyotime Biotechnology Inc. (Shanghai, China). CCK-8 cytotoxicity assay kit was from Meilun Biotechnology Co., Ltd. (Dalian, China). Cell trackers CMFDA and CMTPX were purchased from YEASEN Biotechnology Inc. (Shanghai, China). DMEM, 1× PBS (10 mM, pH 7.4), and BCA protein assay kit were from KeyGen Biotechnology Corp., Ltd. (Nanjing, China).

Apparatus

A microfluidic pressure controller (PreciGenome, PG-MFC-8CH) and a syringe pump (Longer, LSP02−2B, China) were used for the injection of cells and reagents. The bright-field and fluorescence images were obtained with an inverted fluorescence microscope (Leica, DMi8, Germany) equipped with a color digital camera (Leica, DFC550, Germany). CL imaging was performed with a chemiluminescence analyzer (Tanon-5200, China) or UVP imager (BioSpectrum 615 Imaging System). CL kinetic curves were obtained on the MPI-2 multifunctional electrochemical and chemiluminescent analytical system (Xi'an Remex Analytical Instrument Co., Ltd. China). All CL signals were collected under absolute darkness, and CL imaging was performed in cumulative exposure mode.

Chip Fabrication

For the fabrication of the μCLII chip, negative photoresist SU-8 3025 was first spin-coated onto a 4 in. silicon wafer (heated at 120 °C for 10 min before use) fixed on the homogenizers. Meanwhile, the chrome mask for microchamber arrays was adsorbed on a mask holder that was aligned on the nanoimprinting system MA6-SCIL (SÜSS MicroTec SE, Garching, Germany) by negative pressure. Then, the SU-8 3025 coated silicon wafers were put on the chrome mask to obtain the array-patterned silicon wafer molds by soft baking, 365 nm ultraviolet (UV) exposure, post-exposure baking, developing and hard baking, hydrophobically treated with 0.7% 1H, 1H, 2H, 2H-perfluorooctyltrichlorosilane/GH-135 (v/v) solution, and dried at 95 °C for 5 min to facilitate mold release. The formed silicon wafer molds were poured or spin-coated with PDMS. To obtain the microchamber array chip, the PDMS was prepared by mixing PDMS prepolymer and curing agent at a mass ratio of 10:1 to remove the bubbles with evacuation and cured at 80 °C for 30 min. The cured PDMS was peeled from the mold, punched, and bonded on a clean glass slide pretreated with oxygen plasma (Harrick, PDC-FMG-2) to obtain the μCLII chip. Prior to use, the microarray chips were processed by sterilizing in an autoclave, impregnating fully with 1× PBS solution and blocking with 0.1% bovine serum albumin (BSA).

Simulation of Channel Flow Field

The laminar flow was modeled using a commercial finite element solver (COMSOL Multiphysics 5.6), and the fluid flow was solved using the incompressible steady-state Navier−Stokes equations.[31] In implementing the "pressure" boundary condition, the mean flow velocity was used at the inlet to calculate the actual velocity profile, ignoring volume forces. The pressure was set to 0, the backflow was suppressed at the outlet, and the other boundaries were considered as no-slip walls. An ordinary physical field control grid was used for the simulations.

The gas−liquid two-phase flow was controlled by the Cahn−Hilliard equation.[32] The diffusion interface between two immiscible fluids was defined as the region of the dimensionless phase field variable digamma from −1 to 1. In the current model, air with a flow rate of 0.001 m s^{-1} was defined as fluid 1, and water with a density of 998 kg m^{-3} and a kinetic viscosity of 1.003 mPa·s was defined as fluid 2. A step function concerning time was set to control the sequence of fluid injection. The solution diffusion from the addition channel with a contact angle of $\pi/4$ into the CLII microchamber was modeled by the convection-diffusion equation:[33]

$$\frac{\partial c}{\partial t} + \nabla\cdot(-D\nabla c) = R - u\cdot\nabla c \quad (1)$$

where c is the concentration (mol m^{-3}), t is the time, D is the diffusion coefficient (m^2 s^{-1}), R is the reaction rate (mol m^{-3} s^{-1}) that is set to 0 in this work, and $\boldsymbol{u}$ is the flow velocity (m s^{-1}).

Reaction Solution for PRA

The PRA reaction solution was prepared by mixing PCSK9-D1 (1 μg mL^{-1}), IgG Ab-D2 (1 μg mL^{-1}), Block/T2 (100 nM), cDNA (3 μM), RCA solution, and 1× PBS in the volume ratios of 10:10:10:5:21:34. PCSK9-D1 and IgG Ab-D2 were synthesized according to the previous study,[34] and their concentrations were calibrated by BCA protein assay kit. Block/T2 was prepared by mixing Block (10 μM) and T2 (10 μM) in a ratio of 1:1 to anneal at 95 °C for 5 min. cDNA was prepared through a ligation reaction.[35] RCA solution was prepared by mixing phi 29 DNA polymerase (10 U μL^{-1}), dNTPs (10 mM dATP, dGTP, dCTP, and dTTP), recombinant albumin (20 mg mL^{-1}), and phi 29 DNA pol reaction buffer in the volume ratios of 5:5:1:10.

Detection of PCSK9-mAb on μCLII Chip

After 3 μL of the sample containing different concentrations of PCSK9-mAb was mixed with 27 μL of PRA reaction solution, the mixture was injected to fill the chip, and air was then introduced into both addition and capture channels to form individual air-encased-liquid microchambers. After 30 min of incubation, CL detection solution (Supporting Information) was injected into the microchambers from the addition channel to incubate for 5 min, and then 10 mM H_2O_2 was injected to collect the CL images with an exposure time of 20 min. The CL intensities within circles with a given radius were automatically read out by Visionworks (Analytik Jena, Germany) and TanonImage (Tanon, China) software.

Cell Screening with μCLII Chip

After heterogeneous cells dispersed in DMEM (~1×10^6 cells mL^{-1}) containing PRA reaction solution were injected into the μCLII chip at a flow rate of 0.5 μL min^{-1} for single-cell capture, air was injected through the addition and capture channels to form individual air-encased-liquid microchambers and achieve single-cell isolation. After 30 min of culture, the CL detection solution (Supporting Information) was injected through the addition channel to incubate for 5 min. Afterward, 10 mM H_2O_2 was injected to screen the HSHCs with μCLII.

Cell Staining

After the cells were washed three times with DMEM, cell staining with CMFDA or CMTPX was performed by incubating the cells in 5 μM CellTrace Green CMFDA (λ_{ex}492/λ_{em}517 nm) or 2 μM CellTrace Red CMTPX (λ_{ex}577/λ_{em}602 nm) for 20 min. The stained cells were resuspended in DMEM and counted by a cell counter (Countess II, Thermo Fisher Scientific Inc.).

Statistical Analysis

Statistical analyses were performed using Origin (Pro) (version 2021, OriginLab Corporation). All data were expressed as mean ± SD. Statistical significance was assessed using one-way analysis of variance (ANOVA) for analyzing three or more groups. The probability value (P value) < 0.05 was considered statistically significant.

https://doi.org/10.1021/acs.analchem.5c07461
Anal. Chem. 2026, 98, 2541−2549

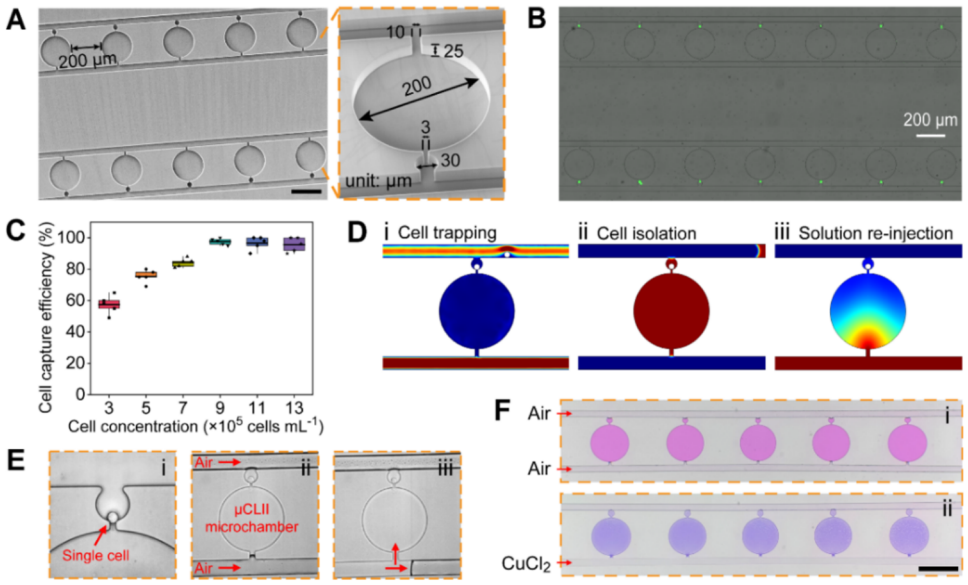

Figure 1. (A) SEM image of microchamber array. The enlarged image is a lantern-shaped microchamber taken at a tilt angle of 45°. Scale bar, 200 μm. (B) Photo of CMFDA-stained cells captured in the trap on the μCLII microchamber array chip. Scale bar, 200 μm. (C) Cell capture efficiency at a capture time of 10 min. Error bars: mean ± SD, n = 5. (D, E) Fluid dynamic simulation (D) and optical micrographs (E) of single-cell trapping (i), cell isolation (ii), and solution reinjection (iii) on the chip. (F) Solution reinjection to air-encased-liquid microchambers on the chip. Images of the air-encased-liquid microchambers filled with Rhodamine B were obtained by dual-side air injection (i) and single-side injection of $CuCl_2$ into (i) (ii). Scale bar, 200 μm.

RESULTS AND DISCUSSION

Working Principle of Cell Screening on μCLII

The μCLII screening of HSHCs relied on the quantitative chemiluminescence immunoimaging detection of the single-cell secreted antibodies, which was performed on a lantern-shaped μCLII array chip with 6 × 50 microchamber array units (Figure S1). The cell capture in traps of lantern-shaped microchamber was based on the differential flow resistance principle, in which the fluid resistance of the trap (Path 1) was lower than that of the channel (Path 2) (Scheme 1B-i). The trapped cell would act as a plug to obstruct the trap lane and prevent subsequent cells from being captured, thereby ensuring single-cell capture in each trap (Scheme 1B-ii). Subsequent injection of air in the channel could lead to the isolation of a single cell to secrete mAbs for CLII detection by forming an air-encased-liquid microchamber (Scheme 1B-iii). Finally, the CL substrate solution was injected from the addition channel for CL imaging analysis (Scheme 1B-iv).

In μCLII, the single-cell secreted antibodies were detected by a homogeneous PRA strategy. The secreted antibody was first recognized by two recognition probes, antigen-DNA1 (Ag-D1) and IgG Ab-DNA2 (IgG Ab-D2), to form a proximity hybridization sequence. After a strand displacement reaction of the formed sequence with Block/T2 hybrid, T2 was released to initiate an RCA reaction for continuously disassembling the dimer of hemin (P1/P2) through another strand displacement reaction, which activated abundant hemin-DNA switches to catalyze the oxidation of luminol by H_2O_2 for producing a strong CL signal (Scheme 1C).

Characterization of the μCLII Chip

The asymmetric lantern shape as well as the spacing distance among CLII chambers, the size of the cell capture trap, and the connection lane between the chamber and the trap were meticulously tailored to meet efficient single-cell capture, maintenance of cell viability, and high resolution enough for CL imaging without cross-talk. The microchambers' diameter and their spacing distance were optimized to be 200 μm, respectively (Figures 1A and S2). The paired configuration of a small cell capture trap (30 μm in diameter) with a large μCLII microchamber enabled both efficient single-cell capture and adequate retention of the culture medium around captured cells, thereby maintaining cell viability throughout the screening process. The total volume of each microchamber was calculated to be 800 picoliter (Figure S3). The cell capture capability of the μCLII chip was demonstrated with green fluorescent dye CMFDA-stained 3H2 hybridomas, and the results showed that ∼100% of captured cells were in the trap (Figure 1B). At a cell concentration of 9 × 10^5 cells mL^{-1}, this chip exhibited a cell capture efficiency of ∼96%, and the single-cell capture efficiency was >80% (Figure 1C). The captured cells showed good cell viability (Figure S4), ensuring subsequent cell screening and mAb production.

Additionally, the formation, stability, and solution reinjection of the air-encased-liquid microchamber array on μCLII chips were investigated. After injecting the dispersion of heterogeneous cells into the chip, single cells could be captured in the traps of individual microchambers, which were then isolated by injecting air into the addition and capture channels (Figure 1D,E) to secrete the specific mAbs through 30 min incubation. The air-encased-liquid microchamber array and formed droplets on the μCLII chip showed good uniformity, high stability, and excellent interassay repeatability. The droplet integrity in microchambers could be maintained over 60 min (Figures S5 and S6). The fast solution reinjection into microchambers could be achieved through the addition channel under maintaining air pressurization in the capture channel (Figure 1D−F).

https://doi.org/10.1021/acs.analchem.5c07461
Anal. Chem. 2026, 98, 2541−2549

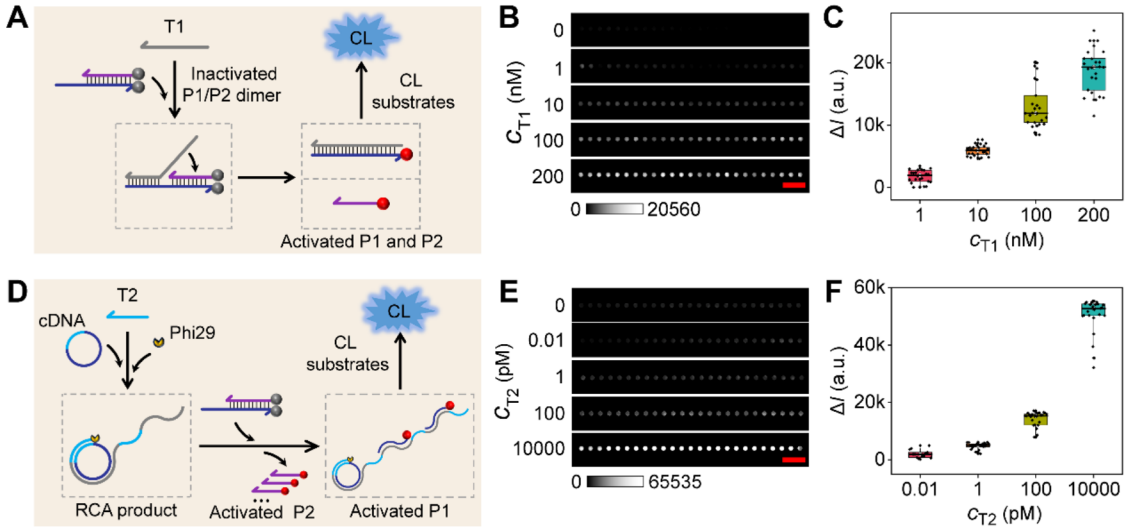

Figure 2. (A) Schematic diagram of T1 detection with hemin-DNA switch. (B) CL images of T1 at different concentrations on the microchamber chip. Scale bar, 1 mm. (C) Box diagram of ΔI vs T1 concentration on the microchamber chip. T1 concentration was calculated as its final concentration in the reaction solution. A total of 25 data points were collected on the microchip. Error bars: mean ± SD, n = 25. (D) A schematic diagram of T2 detection with hemin-DNA switch after RCA reaction. (E) Chemiluminescence images of T2 at different concentrations on the microchamber chip. Scale bar, 1 mm. (F) Box diagram of ΔI vs T2 concentration on the microchamber chip. T2 concentration was calculated as its final concentration in the reaction solution. A total of 25 data points were collected on the microchip. Error bars: mean ± SD, n = 25.

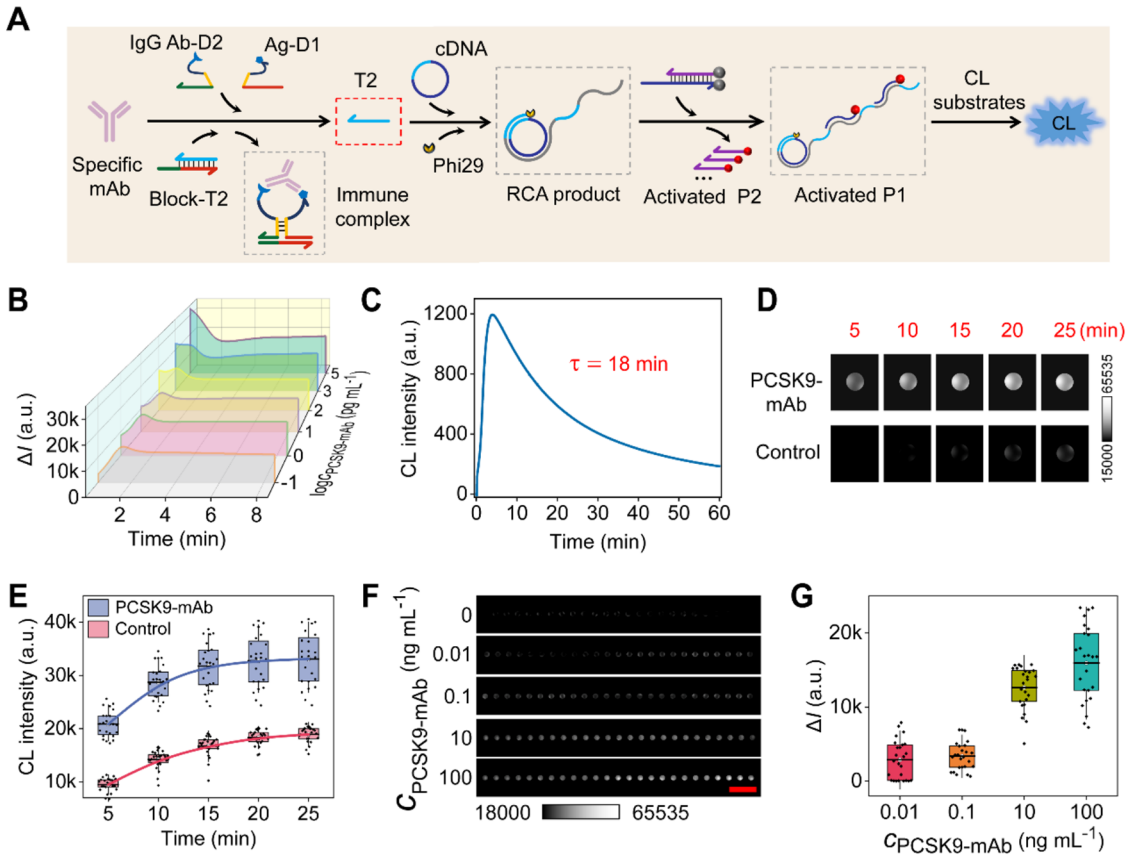

Figure 3. (A) Schematic diagram of antibody detection. (B) CL intensity−time curves for PCSK9-mAb at different concentrations. (C) CL intensity−time curve at 100 ng mL^{-1} PCSK9-mAb for CL lifetime measurement. (D, E) CL images (D) and cumulative CL intensities (E) of 100 ng mL^{-1} PCSK9-mAb and control with different accumulation times. A total of 25 data points were collected on the microchip; each box represents the mean. Error bars: mean ± SD, n = 25. (F) CL images of PCSK9-mAb at different concentrations on the μCLII microchamber array chip. Scale bar, 1 mm. (G) Box diagram of ΔI vs PCSK9-mAb concentration. A total of 25 data points were collected on the microchip. Error bars: mean ± SD, n = 25.

https://doi.org/10.1021/acs.analchem.5c07461
Anal. Chem. 2026, 98, 2541−2549

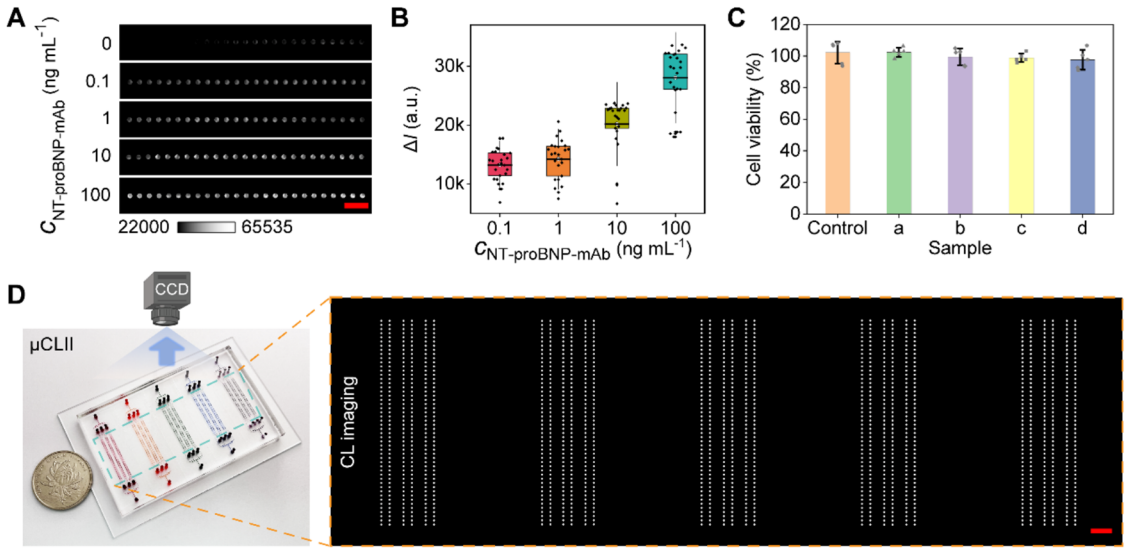

Figure 4. (A) Chemiluminescence images of NT-proBNP-mAb at different concentrations. Scale bar, 1 mm. (B) Box diagram of ΔI vs NT-proBNP-mAb concentration. A total of 25 data points were collected on the microchip. Error bars: mean ± SD, n = 25. (C) Cytotoxicity of reagents used in μCLII toward 6A6 hybridoma cells: 70 min incubation in PRA reaction solution (a), 30 min exposure to CL detection solution (b), 30 min treatment in 200 μM H_2O_2 (c), and sequential 40 min incubation in PRA reaction solution followed by 30 min treatment in a mixture of CL detection solution and 200 μM H_2O_2 (d). The cell cytotoxicity assay was performed with cell proliferation and CCK-8 toxicity test kit according to the manufacturer's recommendation. Data are presented as mean ± SD, n = 5. (D) The wide field CL imaging photo of 5 chips. Scale bar, 2 mm.

Feasibility of Hemin-DNA Switch on μCLII Chip

As the hemin-DNA switch was designed based on the activation of P1 and P2 from the inactivated P1/P2 dimer through a strand displacement reaction, we first verified the feasibility of the hemin-DNA switch by using an ssDNA sequence T1 and P1/P2 dimer on both a 96-well plate and the lantern-shaped microchamber array chip (Figure 2A). When P1 and P2 were in double-stranded hybridization (P1/P2), hemin would be in a dimeric state, and its peroxidase catalytic activity was inhibited, emitting weak CL intensity. The intensities increased with the increasing T1 concentrations from 25 to 125 nM on the 96-well plate and 1−200 nM on the microchamber chip, respectively (Figures 2B,C and S7). Similarly, the RCA reaction-amplified CL response was demonstrated with the T2 sequence and a circle DNA (cDNA) (Figure 2D), which reduced the minimum detectable concentrations of DNA by 5 orders of magnitude on both plate and chip (Figures 2E,F and S8).

Antibody Detection Performance of μCLII

The detection performance of μCLII based on the PRA strategy was studied by using PCSK9-mAb (a lipid-lowering drug) as a model antibody. The recognition probes of PCSK9-D1 and IgG Ab-D2 were synthesized by covalently binding thiolated-DNA on the PCSK9 protein and IgG Ab via the SMCC linker and characterized by PAGE and protein silver staining analysis (Figure S9). For antibody detection, the target PCSK9-mAb was first mixed with PCSK9-D1, IgG Ab-D2, Block/T2, cDNA, and RCA solution (Figure 3A). After incubation for 30 min to perform PRA, a CL detection solution containing P1/P2 dimer and luminol was added to the PRA mixture to initiate the hemin-DNA switches by incubation for 5 min, and then H_2O_2 was injected to collect the CL images. Interestingly, the hemin-DNA-catalyzed luminol-H_2O_2 system showed glow-type CL emission with a luminescence lifetime of 18 min (Figure 3B,C), which was conducive for weak signal acquisition. The CLII detection of PCSK9-mAb was first investigated on a 96-well plate. At an exposure time of 1 min, the PRA-CLII method showed a good linear relationship between relative CL intensity (ΔI, referring to the absolute signal subtracting the background) and linear detection range of PCSK9-mAb in 1.0 fg mL^{-1} to 50 pg mL^{-1} (Figure S10), indicating the feasibility of the proposed PRA-CLII method for highly sensitive detection of low-concentration antibody.

For the detection of PCSK9-mAb on the μCLII chip, the exposure time of CL imaging collection was first evaluated. By considering both the on-chip signal and the noise at different accumulation times, an exposure time of 20 min was selected for μCLII (Figure 3D,E). At the optimized conditions, the μCLII method achieved the quantitative imaging detection of PCSK9-mAb ranging from 0.01 to 100 ng mL^{-1} (Figure 3F,G). The μCLII exhibited good target universality. It could be conveniently applied for NT-proBNP-mAb detection by using corresponding recognition probes, NT-proBNP-D1 (Figure S11) and IgG Ab-D2. The results also showed a good linear relationship between ΔI and the NT-proBNP-mAb concentration ranging from 1 to 100 ng mL^{-1} (Figure 4A,B). In addition, the typical CCK-8 assay results indicated that both the reagents and the μCLII detection did not affect the cell viability (Figure 4C), assuring the activity of the selected HSHCs for mAb production.

The μCLII allowed for high-throughput detection through simultaneous imaging of multiple parallel chips in a single operation. The wide field imaging of 5 chips showed a good signal consistency, with a mean relative standard deviation (RSD) of 10% for the intensity of 1500 detection chambers (Figure 4D).

Screening of High-Yield 6A6 Hybridoma Cells by μCLII

On μCLII, the screening of high-producing hybridoma cells was implemented by quantitatively detecting single-cell secreted antibodies through PRA in independent micro-chambers (Figure 5A). The specificity of μCLII detection for

https://doi.org/10.1021/acs.analchem.5c07461
Anal. Chem. 2026, 98, 2541−2549

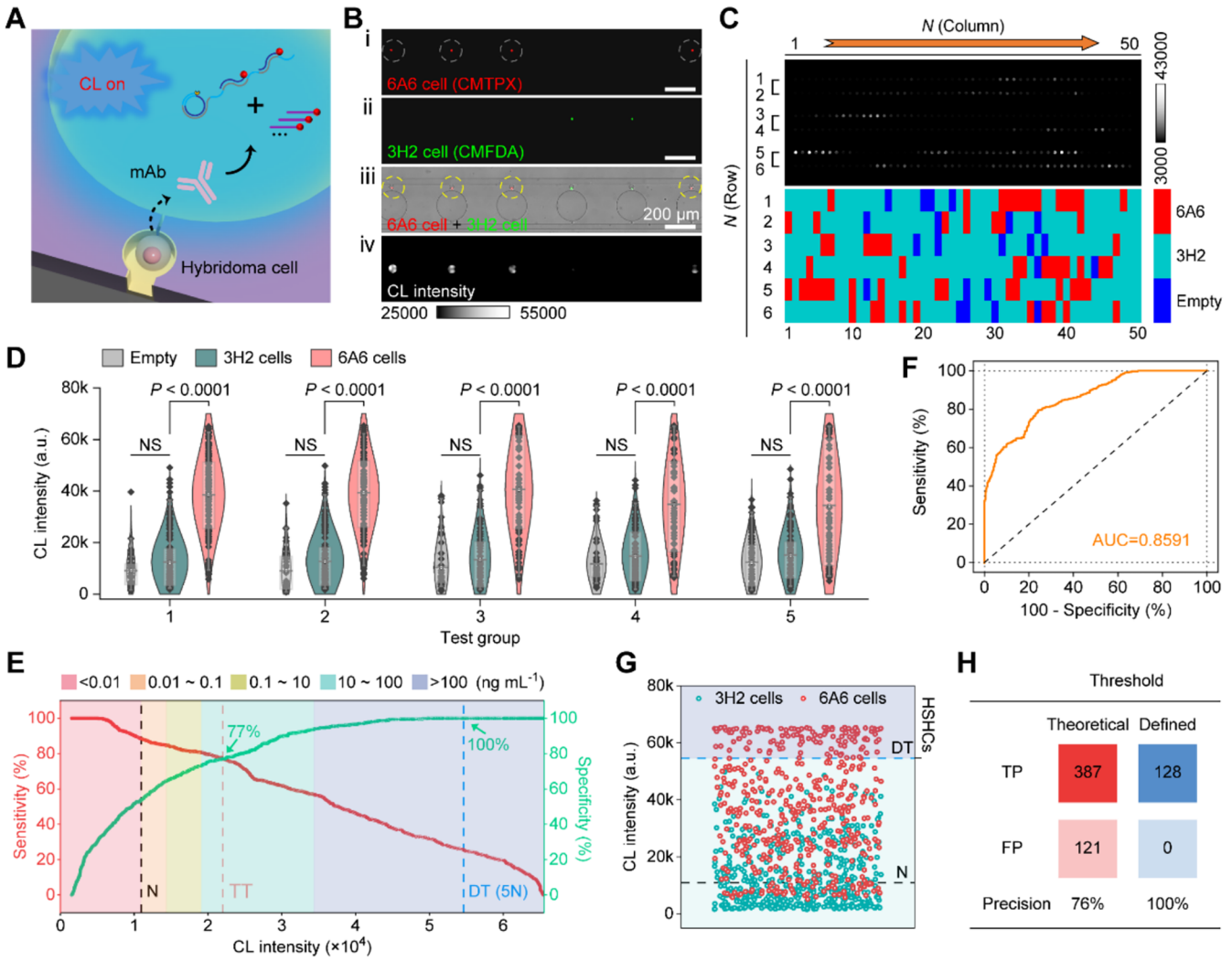

Figure 5. Evaluation of the antibody secretion ability of hybridoma cells by μCLII. (A) A schematic diagram of μCLII detection of single-cell secreted mAb. (B) Fluorescent images of stained 6A6 (i), 3H2 cells (ii), their merge with bright field (iii) in cell capture traps with a diameter of 30 μm, and CL imaging photo of the corresponding μCLII microchambers with a diameter of 200 μm (iv) after secretion for 45 min. (C) μCLII photo of a microchamber array chip injected with the mixture of stained 6A6 and 3H2 cells after 45 min secretion, along with the corresponding fluorescence localization map. (D) Scattered dots, violins, and box plots of μCLII intensities from empty, 3H2, and 6A6 cells on 5 chips for 45 min secretion. Each dot represents a microchamber. Statistical analysis was performed using one-way ANOVA with Tukey's test (NS, not significant). (E) Typical sensitivity and specificity curves of μCLII detection. N, empty intensity; 5N, 5-fold empty intensity, which was defined as threshold (DT); TT, theoretical threshold. (F) ROC curve of the μCLII for discrimination of 3H2 and 6A6 cells. (G) Selection of HSHCs by μCLII with DT. (H) Precision comparison with TT and DT. The precision was calculated from TP/(TP + FP). TP, true positive; FP, false positive.

single-cell secreted antibody was verified with a mixture of commercial 6A6 and 3H2 hybridoma cells, which can secrete PCSK9-mAb and NT-proBNP-mAb, respectively. Using PCSK9-D1 and IgG Ab-D2 as the recognition probes, the microchambers capturing 6A6 cells, which were confirmed by the fluorescent imaging of CMTPX-stained 6A6 and CMFDA-stained 3H2 cells, showed a strong CL signal (Figures 5B,C and S12). The statistical analysis of 5 independent chips showed significantly higher CL intensity from 6A6 cell-captured chambers than that from both 3H2 cell-captured and empty chambers (Figure 5D), demonstrating good specificity of the μCLII method. The similarity of violin plots and CL intensity distributions among 5 chips for the same types of chambers suggested good reproducibility of μCLII detection. The sensitivity and specificity curves gave an optimal theoretical threshold (TT) of CL intensity at 22,000 (Figure 5E), at which the μCLII detection of PCSK9-mAb showed the sensitivity, specificity, accuracy, and precision of 77.09%, 77.00%, 77.04%, and 76.18%, respectively (Figure S13), and a receiver operating characteristic (ROC) graph with an area of 85.91% under the curve (AUC) (Figure 5F), indicating good reliability of μCLII for discrimination of 3H2 and 6A6 cells. To ensure the screening accuracy and high activity of the selected HSHCs, the CL intensity at 100% specificity was defined as the real signal threshold (DT) (Figure 5E), where the CL intensity was 5-fold blank intensity, which was equivalent to the average CL intensity for empty chambers (Figure 5G). With the DT value, the screening of HSHCs showed a precision of 100% (Figure 5G,H), and the concentrations of PCSK9-mAb secreted from the selected HSHCs in 800 pL microchambers were calculated to be >100 ng mL^{-1}, demonstrating high mAb production. It should be noted that when screening the cells with different secretion characteristics, such as different hybridoma cell lines, primary

https://doi.org/10.1021/acs.analchem.5c07461
Anal. Chem. 2026, 98, 2541−2549

B-cells, and heterogeneous hybridoma cells prepared by polyethylene glycol or electrofusion,[36] it was necessary to obtain corresponding sensitivity−specificity curves and determine the DT values at 100% specificity.

The proliferation and mAb production abilities of the selected HSHCs were further evaluated by retrieving them from the μCLII chip with a pressure-based mechanism that utilized an additional elastic film beneath the microchambers (Figure S14). The selected HSHCs not only maintained good viability and proliferated to form stable colonies (Figure S15A) but also exhibited a markedly higher mAb yield compared with that of unscreened cells (Figure S15B), collectively demonstrating the feasibility of the μCLII screening method.

CONCLUSION

A highly sensitive microfluidic CL immunoimaging method for precise screening of HSHCs has been designed by detecting single-cell secreted antibodies on a specially designed lantern-shaped microchamber array chip. In μCLII, the designed lantern-shaped microchamber achieves a high efficiency of single-cell capture in the traps based on the differential flow resistance principle. The homogeneous PRA-based μCLII procedure can be smoothly performed by injecting the cell sample containing PRA reaction solution, forming the individual air-encased-liquid microchambers and reinjecting the CL substrates to simultaneously initiate an on-chip proximity hybridization and RCA reaction for turning on abundant hemin-DNA switches to catalyze the oxidation of luminol by H_2O_2, which produces a strong CL signal to meet the need in sensitivity for cell-secreted antibody detection on a microfluidic chip. Using PCSK9-mAb as a model, this method achieves an excellent screening precision of high-yield anti-PCSK9 hybridomas and thus provides a promising technique for the rapid screening of HSHCs and high-purity mAb production.

ASSOCIATED CONTENT

Supporting Information

The Supporting Information is available free of charge at https://pubs.acs.org/doi/10.1021/acs.analchem.5c07461.

Experimental details for CL imaging detection on 96-well plate and CL imaging assay of T1 and T2 on chip; a schematic diagram of lantern-shaped μCLII microchamber array chip; design and dimensional optimization of the lantern-shaped microchamber; characterization of lantern-shaped structure; viability of captured cells on chip; formation of air-encased-liquid microchamber array on chip; stability of air-encased-liquid microchambers on chip; verify hemin switch; verify the RCA reaction-triggered hemin switch; gel electrophoresis analysis of PCSK9-D1 and IgG Ab-D2; CL detection of PCSK9-mAb on 96-well plate; characterization of NT-proBNP-D1; enlarged images of microchambers; confusion matrix analysis; cell retrieval; proliferation and mAb production ability of the selected high-yield specific hybridoma cells; oligonucleotide sequences (PDF)

AUTHOR INFORMATION

Corresponding Authors

Jie Wu − *State Key Laboratory of Analytical Chemistry for Life Science, School of Chemistry and Chemical Engineering, Nanjing University, Nanjing 210023, China;* orcid.org/0000-0003-1379-122X; Email: wujie@nju.edu.cn

Huangxian Ju − *State Key Laboratory of Analytical Chemistry for Life Science, School of Chemistry and Chemical Engineering, Nanjing University, Nanjing 210023, China;* orcid.org/0000-0002-6741-5302; Email: hxju@nju.edu.cn

Authors

Wencheng Xiao − *State Key Laboratory of Analytical Chemistry for Life Science, School of Chemistry and Chemical Engineering, Nanjing University, Nanjing 210023, China*

Hang Ao − *State Key Laboratory of Analytical Chemistry for Life Science, School of Chemistry and Chemical Engineering, Nanjing University, Nanjing 210023, China*

Nilin Wu − *State Key Laboratory of Analytical Chemistry for Life Science, School of Chemistry and Chemical Engineering, Nanjing University, Nanjing 210023, China*

Jun Sun − *State Key Laboratory of Analytical Chemistry for Life Science, School of Chemistry and Chemical Engineering, Nanjing University, Nanjing 210023, China*

Wenrui Hu − *State Key Laboratory of Analytical Chemistry for Life Science, School of Chemistry and Chemical Engineering, Nanjing University, Nanjing 210023, China*

Yunlong Chen − *State Key Laboratory of Analytical Chemistry for Life Science, School of Chemistry and Chemical Engineering, Nanjing University, Nanjing 210023, China;* orcid.org/0000-0002-3775-3028

Complete contact information is available at: https://pubs.acs.org/10.1021/acs.analchem.5c07461

Author Contributions

†W.X. and H.A. contributed equally to this work. All authors have approved the final version of the manuscript.

Notes

The authors declare no competing financial interest.

ACKNOWLEDGMENTS

This work was financially supported by the National Natural Science Foundation of China (21827812 and 22574076) and the Frontier Technology Research and Development Program of Jiangsu Province (BF2024055).

REFERENCES

(1) Dumontet, C.; Reichert, J. M.; Senter, P. D.; Lambert, J. M.; Beck, A. Antibody−drug conjugates come of age in oncology. *Nat. Rev. Drug Discovery* **2023**, *22*, 641−661.

(2) Beck, A.; Wurch, T.; Bailly, C.; Corvaia, N. Strategies and challenges for the next generation of therapeutic antibodies. *Nat. Rev. Immunol.* **2010**, *10*, 345−352.

(3) Di Cristina, M.; Nunziangeli, L.; Giubilei, M. A.; Capuccini, B.; d'Episcopo, L.; Mazzoleni, G.; Baldracchini, F.; Spaccapelo, R.; Crisanti, A. An antigen microarray immunoassay for multiplex screening of mouse monoclonal antibodies. *Nat. Protoc.* **2010**, *5*, 1932−1944.

(4) Zhang, W.; Li, R.; Jia, F.; Hu, Z.; Li, Q.; Wei, Z. A microfluidic chip for screening high-producing hybridomas at single cell level. *Lab Chip* **2020**, *20*, 4043−4051.

(5) Mazutis, L.; Gilbert, J.; Ung, W. L.; Weitz, D. A.; Griffiths, A. D.; Heyman, J. A. Single-cell analysis and sorting using droplet-based microfluidics. *Nat. Protoc.* **2013**, *8*, 870−891.
(6) Zhang, D.; Xie, C.; Wang, R.; Yang, Q.; Chen, H.; Ling, S.; Wang, S.; Jia, K. Effective preparation of a monoclonal antibody against human chromogranin A for immunohistochemical diagnosis. *BMC Biotechnol.* **2018**, *18*, No. 25.
(7) Ao, H.; Chen, W.; Wu, J.; Xiao, W.; Ju, H. Chemiluminescent screening of specific hybridoma cells via a proximity-rolling circle activated enzymatic switch. *Commun. Biol.* **2022**, *5*, No. 308.
(8) Wang, J.; Song, Q.; Yang, T.; Li, Y.; Zhang, L.; Li, J.; Liu, F.; Lin, Y.; Xu, X.; Heng, Y.; Xu, L.; Zhang, S.; Zhou, J.; Liu, Y.; Kong, L.; Tang, D.; Ji, C.; Tan, B.; Liao, P.; Pan, N.; Yi, W.; Wang, Z. The challenges and breakthroughs in the development of diagnostic monoclonal antibodies. *View* **2024**, *5*, No. 20240017.
(9) Zhang, M.; Zou, Y.; Xu, X.; Zhang, X.; Gao, M.; Song, J.; Huang, P.; Chen, Q.; Zhu, Z.; Lin, W.; Zare, R. N.; Yang, C. Highly parallel and efficient single cell mRNA sequencing with paired picoliter chambers. *Nat. Commun.* **2020**, *11*, No. 2118.
(10) Gao, Y.; Wang, Y.; He, B.; Pan, Y.; Zhou, D.; Xiong, M.; Song, Y. An enzyme-loaded metal-organic framework-assisted microfluidic platform enables single-cell metabolite analysis. *Angew. Chem., Int. Ed.* **2023**, *62*, No. e202302000.
(11) Debs, B. E.; Utharala, R.; Balyasnikova, I. V.; Griffiths, A. D.; Merten, C. A. Functional single-cell hybridoma screening using droplet-based microfluidics. *Proc. Natl. Acad. Sci. U.S.A.* **2012**, *109*, 11570−11575.
(12) Gérard, A.; Woolfe, A.; Mottet, G.; Reichen, M.; Castrillon, C.; Menrath, V.; Ellouze, S.; Poitou, A.; Doineau, R.; Briseno-Roa, L.; Canales-Herrerias, P.; Mary, P.; Rose, G.; Ortega, C.; Delincé, M.; Essono, S.; Jia, B.; Iannascoli, B.; Goff, O. R.-L.; Kumar, R.; Stewart, S. N.; Pousse, Y.; Shen, B.; Grosselin, K.; Saudemont, B.; Sautel-Caillé, A.; Godina, A.; McNamara, S.; Eyer, K.; Millot, G. A.; Baudry, J.; England, P.; Nizak, C.; Jensen, A.; Griffiths, A. D.; Bruhns, P.; Brenan, C. High-throughput single-cell activity-based screening and sequencing of antibodies using droplet microfluidics. *Nat. Biotechnol.* **2020**, *38*, 715−721.
(13) Eyer, K.; Doineau, R. C. L.; Castrillon, C. E.; Briseño-Roa, L.; Menrath, V.; Mottet, G.; England, P.; Godina, A.; Brient-Litzler, E.; Nizak, C.; Jensen, A.; Griffiths, A. D.; Bibette, J.; Bruhns, P.; Baudry, J. Single-cell deep phenotyping of IgG-secreting cells for high-resolution immune monitoring. *Nat. Biotechnol.* **2017**, *35*, 977−982.
(14) Bounab, Y.; Eyer, K.; Dixneuf, S.; Rybczynska, M.; Chauvel, C.; Mistretta, M.; Tran, T.; Aymerich, N.; Chenon, G.; Llitjos, J. F.; Venet, F.; Monneret, G.; Gillespie, I. A.; Cortez, P.; Moucadel, V.; Pachot, A.; Troesch, A.; Leissner, P.; Textoris, J.; Bibette, J.; Guyard, C.; Baudry, J.; Griffiths, A. D.; Védrine, C. Dynamic single-cell phenotyping of immune cells using the microfluidic platform DropMap. *Nat. Protoc.* **2020**, *15*, 2920−2955.
(15) Ansaryan, S.; Liu, Y.-C.; Li, X.; Economou, A. M.; Eberhardt, C. S.; Jandus, C.; Altug, H. High-throughput spatiotemporal monitoring of single-cell secretions via plasmonic microwell arrays. *Nat. Biomed. Eng.* **2023**, *7*, 943−958.
(16) Van Lent, J.; Breukers, J.; Ven, K.; Ampofo, L.; Horta, S.; Pollet, F.; Imbrechts, M.; Geukens, N.; Vanhoorelbeke, K.; Declerck, P.; Lammertyn, J. Miniaturized single-cell technologies for monoclonal antibody discovery. *Lab Chip* **2021**, *21*, 3627−3654.
(17) Xu, Q.-Q.; Jiang, Y.-R.; Chen, J.-B.; Wu, J.; Chen, Y.-X.; Fan, Q.-X.; Wang, H.-F.; Yang, Y.; Pan, J.-Z.; Fang, Q. Single cell-pair proteomics for decoding immune-cancer cell interactions. *Adv. Sci.* **2025**, *12*, No. 2414769.
(18) Ogunniyi, A. O.; Story, C. M.; Papa, E.; Guillen, E.; Love, J. C. Screening individual hybridomas by microengraving to discover monoclonal antibodies. *Nat. Protoc.* **2009**, *4*, 767−782.
(19) Ahmadi, F.; Tran, H.; Letourneau, N.; Little, S. R.; Fortin, A.; Moraitis, A. N.; Shih, S. C. C. An automated single-cell droplet-digital microfluidic platform for monoclonal antibody discovery. *Small* **2024**, *20*, No. 2308950.
(20) Zhang, W.; Li, Q.; Jia, F.; Hu, Z.; Wei, Z. A microfluidic chip for screening and sequencing of monoclonal antibody at a single-cell level. *Anal. Chem.* **2021**, *93*, 10099−10105.
(21) Akhavan-Tafti, H.; Binger, D. G.; Blackwood, J. J.; Chen, Y.; Creager, R. S.; de Silva, R.; Eickholt, R. A.; Gaibor, J. E.; Handley, R. S.; Kapsner, K. P.; Lopac, S. K.; Mazelis, M. E.; McLernon, T. L.; Mendoza, J. D.; Odegaard, B. H.; Reddy, S. G.; Salvati, M.; Schoenfelner, B. A.; Shapir, N.; Shelly, K. R.; Todtleben, J. C.; Wang, G.; Xie, W. A homogeneous chemiluminescent immunoassay method. *J. Am. Chem. Soc.* **2013**, *135*, 4191−4194.
(22) Yamanishi, C. D.; Chiu, J. H.-C.; Takayama, S. Systems for multiplexing homogeneous immunoassays. *Bioanalysis* **2015**, *7*, 1545−1556.
(23) Xiao, Q.; Xu, C. Research progress on chemiluminescence immunoassay combined with novel technologies. *Trac-Trends Anal. Chem.* **2020**, *124*, No. 115780.
(24) Yang, M.; Huang, J.; Fan, J.; Du, J.; Pu, K.; Peng, X. Chemiluminescence for bioimaging and therapeutics: recent advances and challenges. *Chem. Soc. Rev.* **2020**, *49*, 6800−6815.
(25) Liu, Y.; Shen, W.; Li, Q.; Shu, J.; Gao, L.; Ma, M.; Wang, W.; Cui, H. Firefly-mimicking intensive and long-lasting chemiluminescence hydrogels. *Nat. Commun.* **2017**, *8*, No. 1003.
(26) Zheng, T.; Nie, W.; Yu, L.; Shu, J.; Li, Y.; Tian, C.; Wang, W.; Cui, H. A chemical timer approach to delayed chemiluminescence. *Proc. Natl. Acad. Sci. U.S.A* **2022**, *119*, No. e2207693119.
(27) Blau, R.; Shelef, O.; Shabat, D.; Satchi-Fainaro, R. Chemiluminescent probes in cancer biology. *Nat. Rev. Bioeng.* **2023**, *1*, 648−664.
(28) Fan, F.; Shen, H.; Zhang, G.; Jiang, X.; Kang, X. Chemiluminescence immunoassay based on microfluidic chips for α-fetoprotein. *Clin. Chim. Acta* **2014**, *431*, 113−117.
(29) Xiao, Q.; Wu, J.; Dang, P.; Ju, H. Multiplexed chemiluminescence imaging assay of protein biomarkers using DNA microarray with proximity binding-induced hybridization chain reaction amplification. *Anal. Chim. Acta* **2018**, *1032*, 130−137.
(30) Feng, W.; Beer, J. C.; Hao, Q.; Ariyapala, I. S.; Sahajan, A.; Komarov, A.; Cha, K.; Moua, M.; Qiu, X.; Xu, X.; Iyengar, S.; Yoshimura, T.; Nagaraj, R.; Wang, L.; Yu, M.; Engel, K.; Zhen, L.; Xue, W.; Lee, C.-J.; Park, C. H.; Peng, C.; Zhang, K.; Grzybowski, A.; Hahm, J.; Schmidt, S. V.; Odainic, A.; Spitzer, J.; Buddika, K.; Kuo, D.; Fang, L.; Zhang, B.; Chen, S.; Latz, E.; Yin, Y.; Luo, Y.; Ma, X.-J. NULISA: a proteomic liquid biopsy platform with attomolar sensitivity and high multiplexing. *Nat. Commun.* **2023**, *14*, No. 7238.
(31) Qiu, T.; Lee, T.-C.; Mark, A. G.; Morozov, K. I.; Münster, R.; Mierka, O.; Turek, S.; Leshansky, A. M.; Fischer, P. Swimming by reciprocal motion at low Reynolds number. *Nat. Commun.* **2014**, *5*, No. 5119.
(32) Xie, F.; Zheng, X.; Triantafyllou, M. S.; Constantinides, Y.; Zheng, Y.; Karniadakis, G. E. Direct numerical simulations of two-phase flow in an inclined pipe. *J. Fluid Mech.* **2017**, *825*, 189−207.
(33) Wong, S. H.; Ward, M. C. L.; Wharton, C. W. Micro T-mixer as a rapid mixing micromixer. *Sens. Actuator, B* **2004**, *100*, 359−379.
(34) Ren, K.; Wu, J.; Zhang, Y.; Yan, F.; Ju, H. Proximity hybridization regulated DNA biogate for sensitive electrochemical immunoassay. *Anal. Chem.* **2014**, *86*, 7494−7499.
(35) Zhang, R.; Wu, J.; Ao, H.; Fu, J.; Qiao, B.; Wu, Q.; Ju, H. A rolling circle-amplified G-Quadruplex/hemin DNAzyme for chemiluminescence immunoassay of the SARS-CoV-2 protein. *Anal. Chem.* **2021**, *93*, 9933−9938.
(36) Skelley, A. M.; Kirak, O.; Suh, H.; Jaenisch, R.; Voldman, J. Microfluidic control of cell pairing and fusion. *Nat. Methods* **2009**, *6*, 147−152.

https://doi.org/10.1021/acs.analchem.5c07461
Anal. Chem. 2026, 98, 2541−2549